Supplement of

A Phase Separation Inlet for Droplets, Ice Residuals, and Interstitial Aerosol Particles

Libby Koolik et al.

5

Correspondence to: Daniel Cziczo (djcziczo@purdue.edu)

S1   Weber Number Calculations

N_{We} describes the ratio of the Bernoulli pressure caused by surrounding and opposing flow on a falling droplet to the surface tension of the droplet (Pruppacher and Klett, 1997). Droplet disruption has been estimated to occur for N_{We} significantly larger than 10 (Pruppacher and Klett, 1997). The following expression was used to solve for N_{We} and maximum droplet diameter (d_{max}):

$$N_{We} = \frac{\rho_a d_{max} U_\infty^2}{\sigma} \tag{1}$$

$$d_{max} = \frac{8\sigma}{C_D \rho_a U_\infty^2} \tag{2}$$

where ρ_a refers to density of the surrounding air, σ is the surface tension of the droplet, U_∞ is the difference between the droplet velocity and the gas velocity, and C_D refers to the drag coefficient (Pekour and Cziczo, 2011). The droplet velocity was approximated using the following expression from Pekour and Cziczo (2011):

$$\frac{m_p v_i^2}{2} = \frac{m_p v_{i-1}^2}{2} + \Delta x \cdot F_{D_{i-1}} \tag{3}$$

$$F_D = \frac{\pi C_D \rho_a v^2 \chi^2 d_{max}^2}{8 C_c} \tag{4}$$

where C_D refers to the drag coefficient, χ is the shape factor, and C_C is the slip factor.

N_{We} as a function of distance along the L-PCVI was modeled for droplets varying in size from 1 to 75 μm using SPIDER's L-PCVI IF of 50.0 L min^{-1} (Figure S1). The maximum N_{We} calculated was approximately 0.3, signifying that droplets are not expected to break up in the L-PCVI using SPIDER's flow rates.

Ice crystals and supercooled droplets that pass through the L-PCVI enter the droplet evaporation chamber, which utilizes the WBF process. The chamber is held at -16° C because the difference in saturation vapor pressure between water and ice is at maximum. By the end of the chamber, the ice crystals and water droplets exist in two separate size modes (i.e., ice crystals maintain their size while droplets evaporate).

N_{We} was calculated for the PCVI and found to be higher for all droplets than in the L-PCVI due to higher gas velocity (Figure S2). Still, the maximum N_{We} for the largest droplet remained below the threshold of 10, signifying that remaining droplets should not break up before rejection. Note that the 3D printed PCVI (Figure 1) incorporates the Kulkarni et al. (2011) gradual, conical nozzle instead of stepped inlet nozzle.

S2   SPIDER Operating Methodology

The SPIDER startup routine was designed to ensure there is no flow blockage by moving from the bottom to the top of the instrument (i.e., farthest downstream to initial sampling of atmosphere). The first step is to connect the critical communication lines from SPIDER to the computer via USB cables; these include an Arduino UNO, which receives data from the temperature sensors (Figure 2); a splitter (Alicat-BB9), which transmits the flow values of each mass flow controller (MFC); and the aerosol particle and residual measurement devices. Second, the vacuum pump and pressurized air are turned on to provide flows to the MFCs. Next, the PCVI flows are turned on by setting the AF followed by the PF. This starts the flow through the chamber. The last step is to turn on the flows for the L-PCVI, again turning on AF before PF.

At each point in this process, the operator verifies via pressure measurements or achieved flow rates that no flow problems have occurred. Finally, the user turns on the low-temperature cooling bath (Proline RP 1290, Lauda-Koenigshofen) and flushes the chamber with dry, filtered air.

S3   L-PCVI Results Compared to Hiranuma et al. (2016)

Figure S3 overlays the results from this work onto a figure from Hiranuma et al. (2016).

S4   Droplet Evaporation Models

The model of droplet evaporation was based on the equation of evaporation described by Lohmann et al (2016):

$$r(t)=\sqrt{r_o^2+2\left(\frac{S\text{-}1}{F_k+F_d}\right)t} \tag{5}$$

where r_o is the initial droplet radius and S is the supersaturation. F_k and F_d are defined as:

$$F_k=\rho_w\left(\frac{L_v^2}{KR_vT^2}\right) \tag{6}$$

$$F_d=\rho_w\left(\frac{R_vT}{D_ve_{s,w}(T)}\right) \tag{7}$$

where ρ_w is the density of liquid water, L_v is the latent heat of vaporization, D_v is the diffusion coefficient for water vapor in air, $e_{s,w}$ is the saturation vapor pressure of water, and K is the coefficient of thermal conductivity in air. This equation is considered valid for large droplets (larger than 5 μm), as it neglects the effects of solution and curvature of the droplet. When sampling from clouds, the droplets should satisfy this assumption.

The model was run with the approximate chamber dimensions for a variety of initial droplet sizes (5-50 μm) at different system saturations (0.25, 0.5, 0.75, and 1) (Figure S4). In the simulation where $S = 1$, all of the droplets retain their original size. In the other three simulations, the 5 and 12.5 μm droplets fully evaporate by the end of the chamber. The 25 μm droplet evaporates fully when supersaturation is equal to or lower than 0.5.

S5   Additional PCVI Verification Test

An additional PCVI verification test was performed to characterize the rejected particles in the PF. A polydisperse particle flow from the laboratory air was used and the OPS was connected to the SF of the PCVI. Measurements at 1-second resolution were made while the PCVI flows were off to capture the distribution of particles in the input flow

70   (Figure S5a). Next, the OPS was disconnected from the SF and reconnected to the PF and PCVI flows were turned on (PF set to 8.0 L min^{-1} and AF set to 2.5 L min^{-1}) to measure the rejected particles (Figure S5b). Finally, the OPS was reconnected to the SF, and measurement were repeated (Figure S5c). A comparison of Figures S5a and S5b was performed to show the PCVI was functioning correctly. In a functional PCVI, the small particles should be rejected (and pumped away in the PF), so there should be a comparable number of particles in the small bins of the SF when

75   the PCVI flows are off to the number of particles in the small bins of the PF when the PCVI flows are on. The concentrations of particles in the three smallest bins from the operational PCVI's PF (Figure S5b) are within 15% of those recorded when the PCVI flows were off and the OPS was attached in the SF region (Figure S5a). In the bins closest to the expected D50, the concentrations of larger particles in the PCVI's PF (Figure S5b) are much smaller (50%) than the concentrations in the SF when the PCVI flows are off (Figure S5a). It is expected that the

80   concentrations of particles in the PF larger than the theoretical D50 will be significantly smaller than their counterparts in the SF sample because these larger particles are transmitting through the SF of the PCVI with flows on and not being pumped away in the PF.

Additionally, Figure S5d shows the same data as Figure S5a, but with the same scaling as Figure S5c. When the PCVI flows are off (Figure S5d), there are large numbers of small particles that are not seen in the SF when the PCVI flows

85   are on (Figure S5c).

S6   SPL Background Conditions

Meteorological conditions during sampling and background aerosol particle concentration at SPL are shown in Figure S6. Ice crystal residual particle concentration is compared against wind speed for two clear periods in Figure S7.
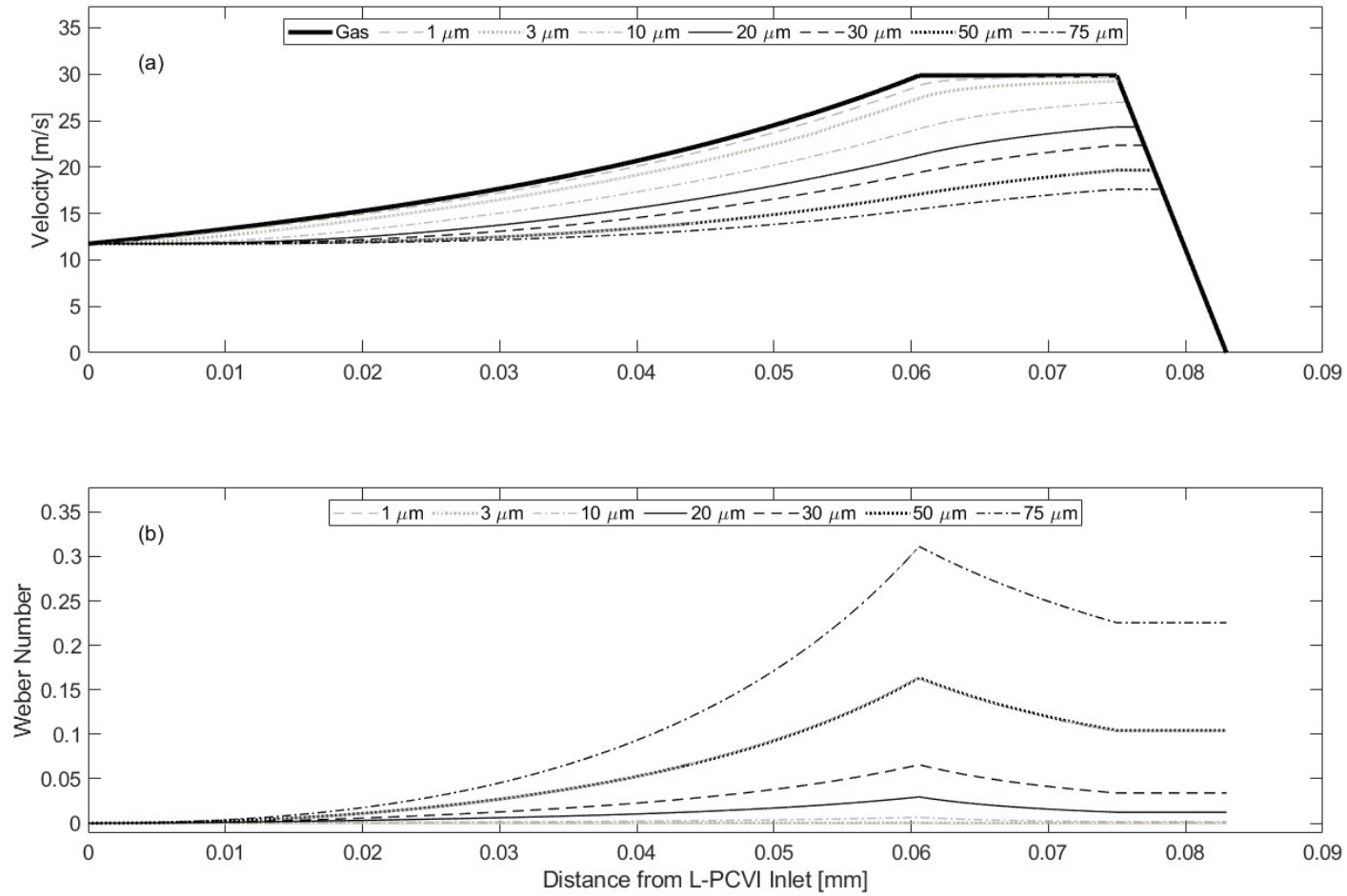
Figure S1: (a) Velocity calculated for droplet sizes and gas shown as a function of distance from the L-PCVI inlet. (b) The corresponding Weber number calculated along the L-PCVI inlet.
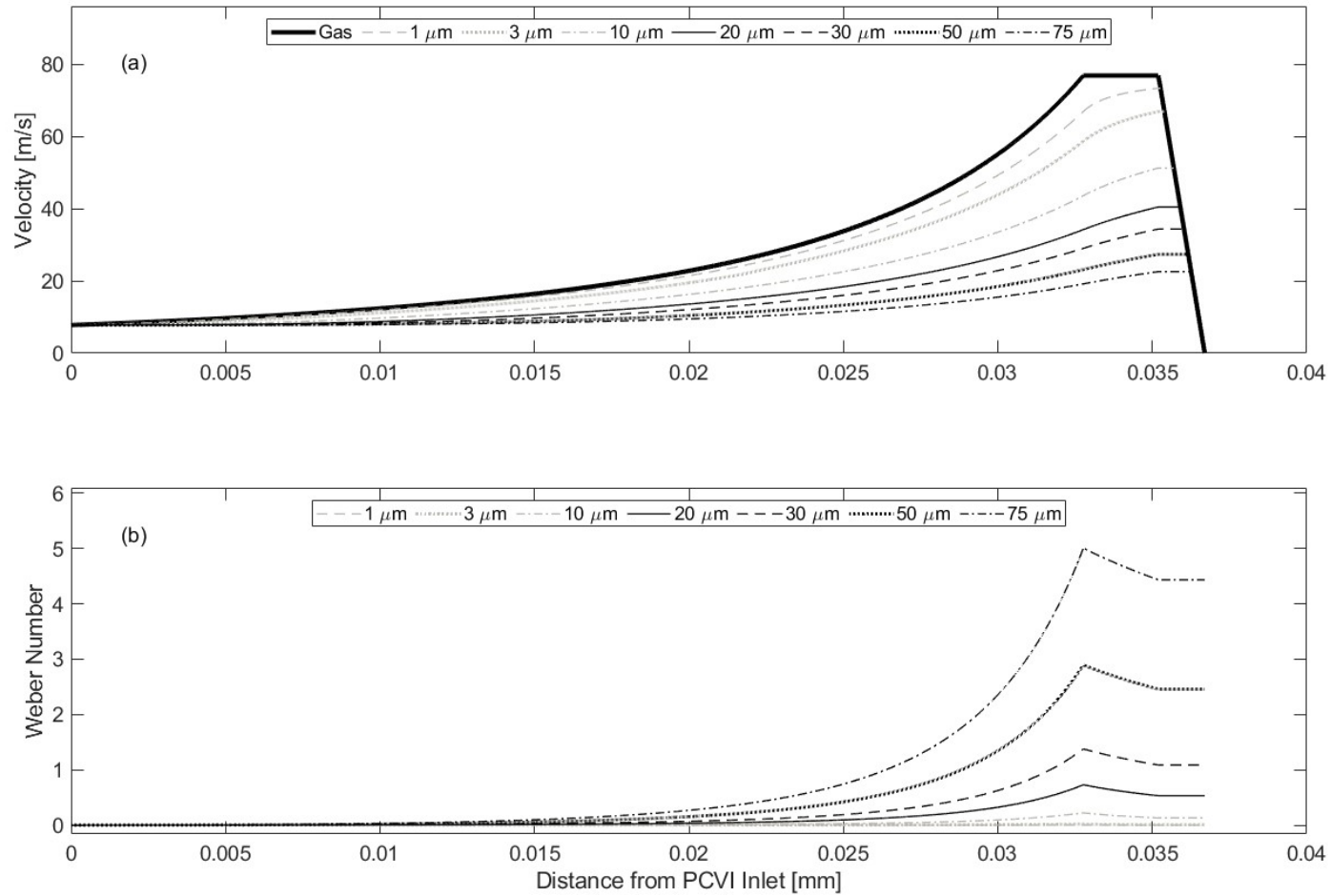
Figure S2: (a) Velocity calculated for droplet sizes and gas shown as a function of distance from the PCVI inlet. (b) The corresponding Weber number calculated along the PCVI inlet.
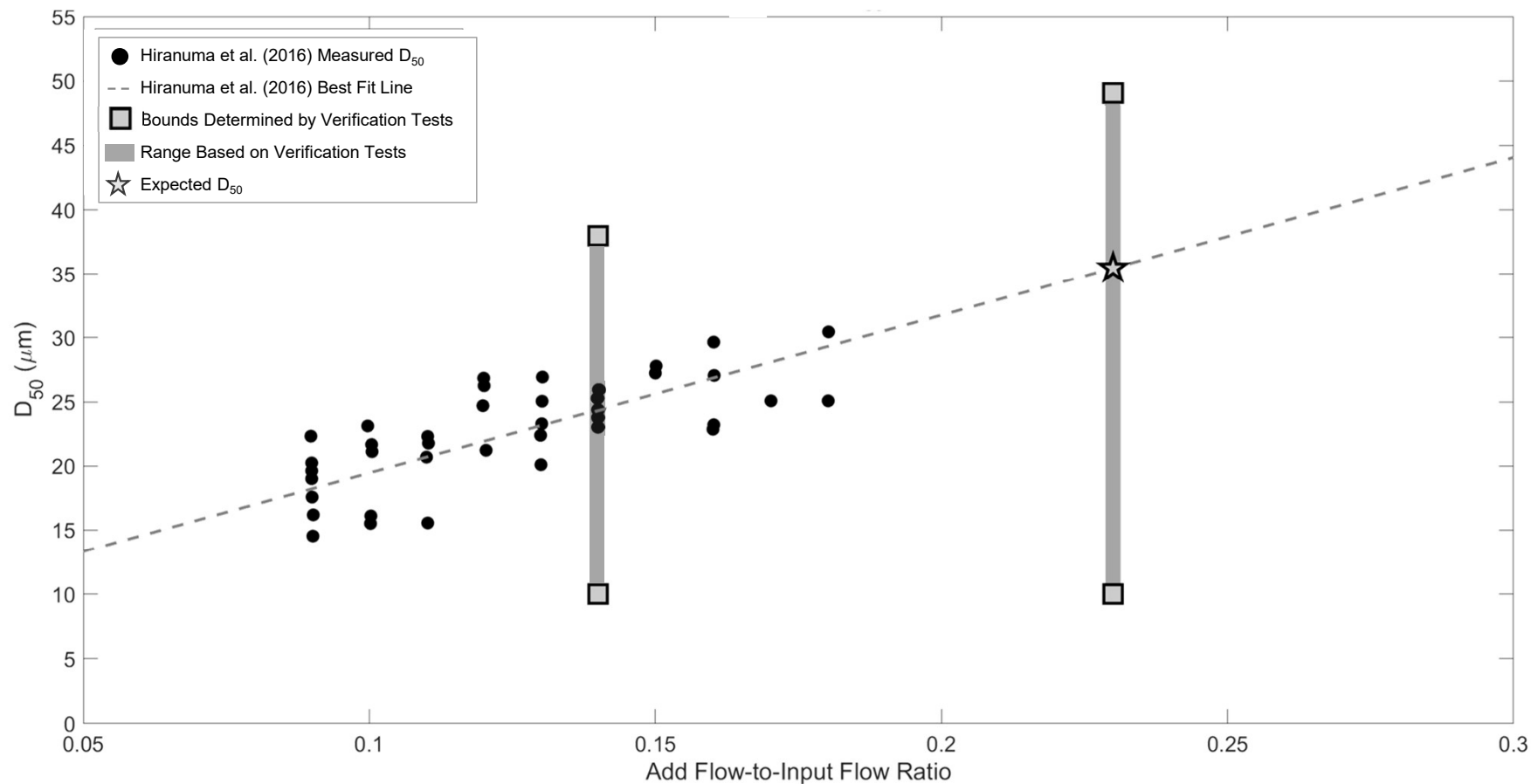
Figure S3: D50 as a function of counterflow to input flow ratio from this work and Hiranuma et al. (2016). The grey dashed line and black points refer to the values from Hiranuma et al. (2016). The gray vertical lines indicate the ranges from the experimental verification tests in this work. The star is the anticipated D50 using SPIDER's flow ratio and the Hiranuma et al. (2016) data fit line.
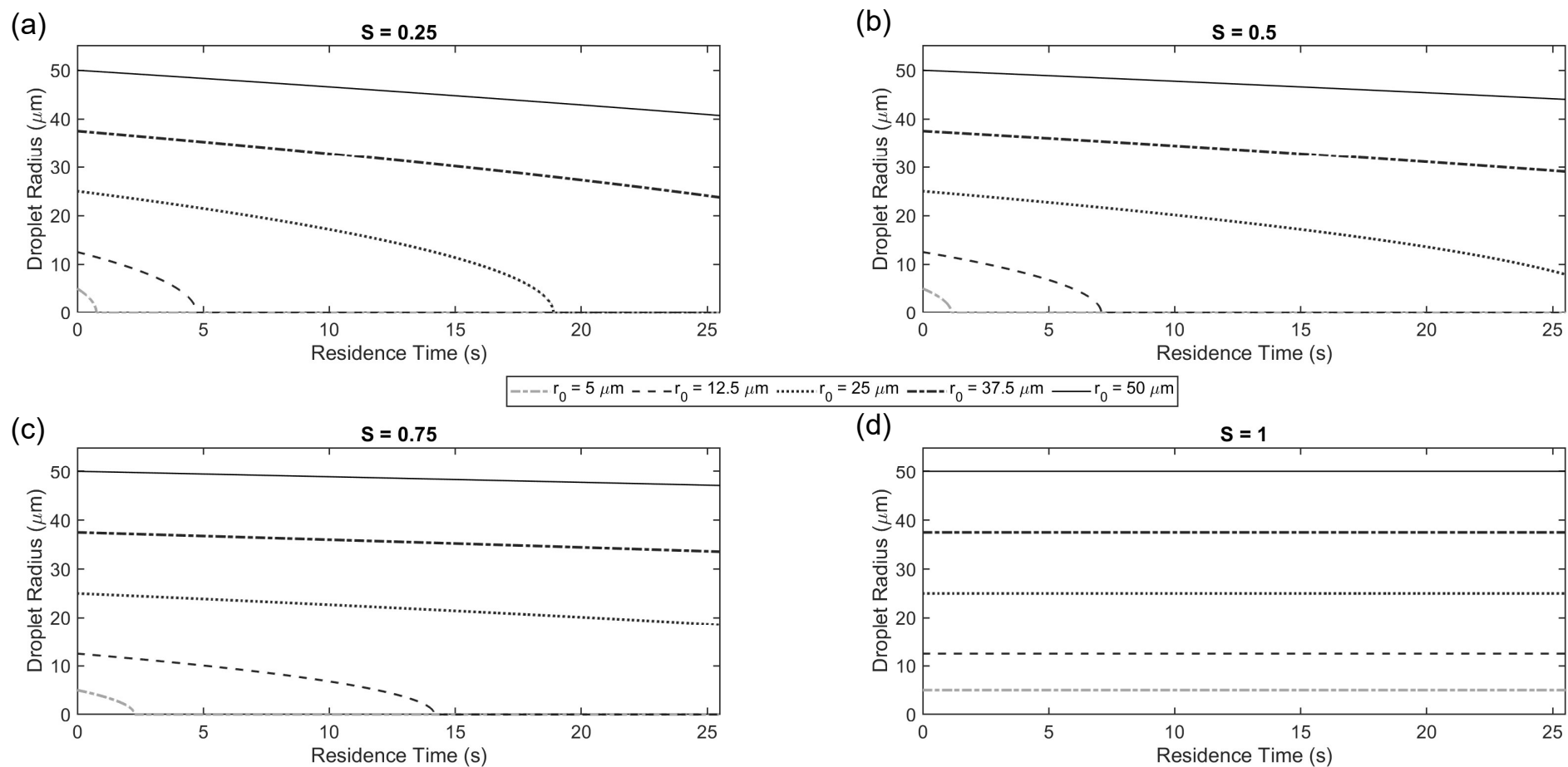
Figure S4: Droplet size, as a function of time (i.e., evaporation time) for five initial droplet sizes relevant to SPIDER for saturation ratios of (a) 0.25, (b) 0.5, (c) 0.75. and (d) 1.0.
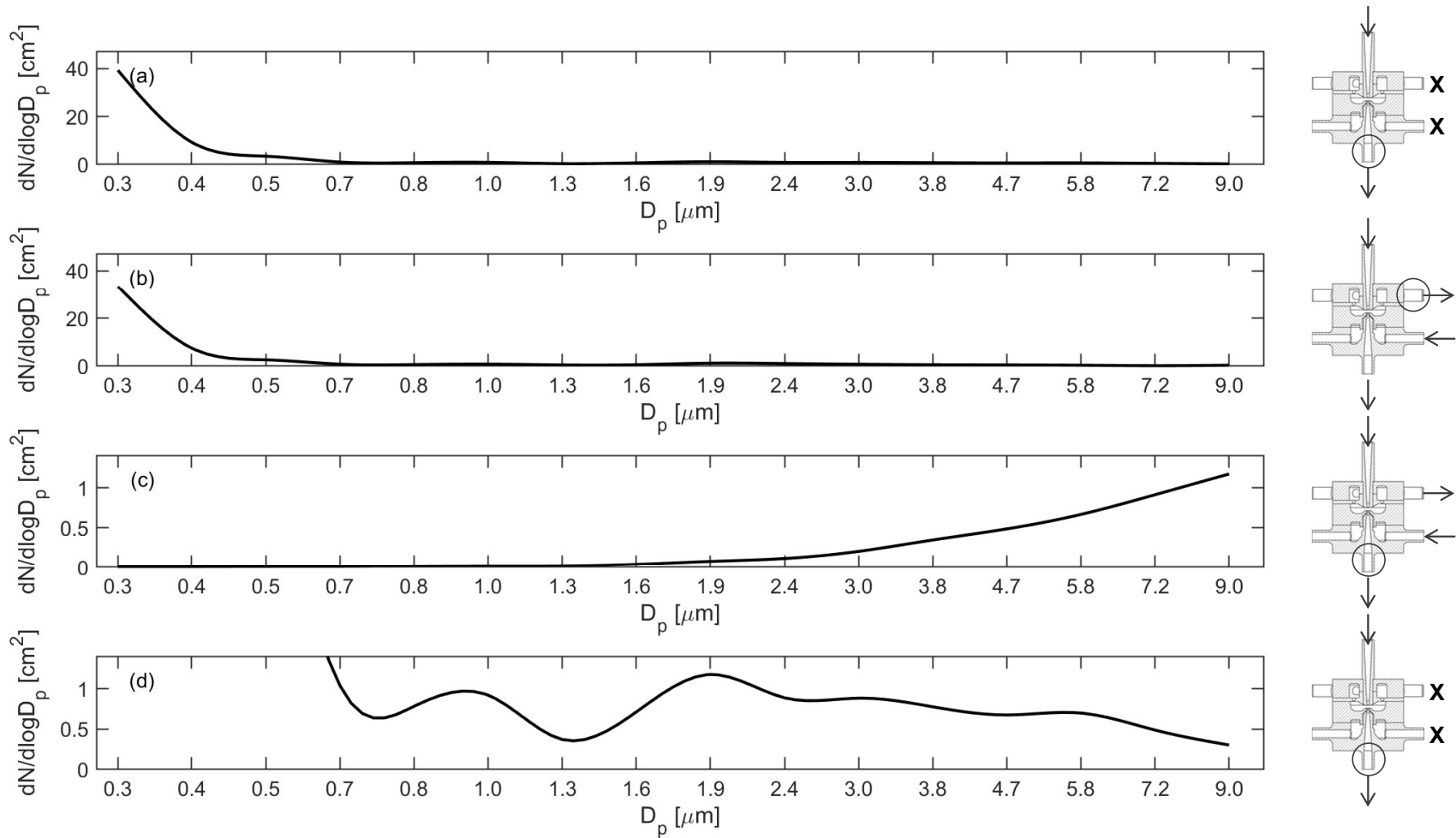
Figure S5: Number concentration as a function of particle diameter for three PCVI verification tests. (a) A control experiment with the PCVI flows turned off with the OPS in the SF. (b) The aerosol concentration for sizes below the PCVI cutpoint with the PCVI flows turned on with the OPS in the PF. (c) The PCVI flows turned on with the OPS in the SF. (d) Panel (a) is reproduced with the same y-axis limits as (c) for comparison.
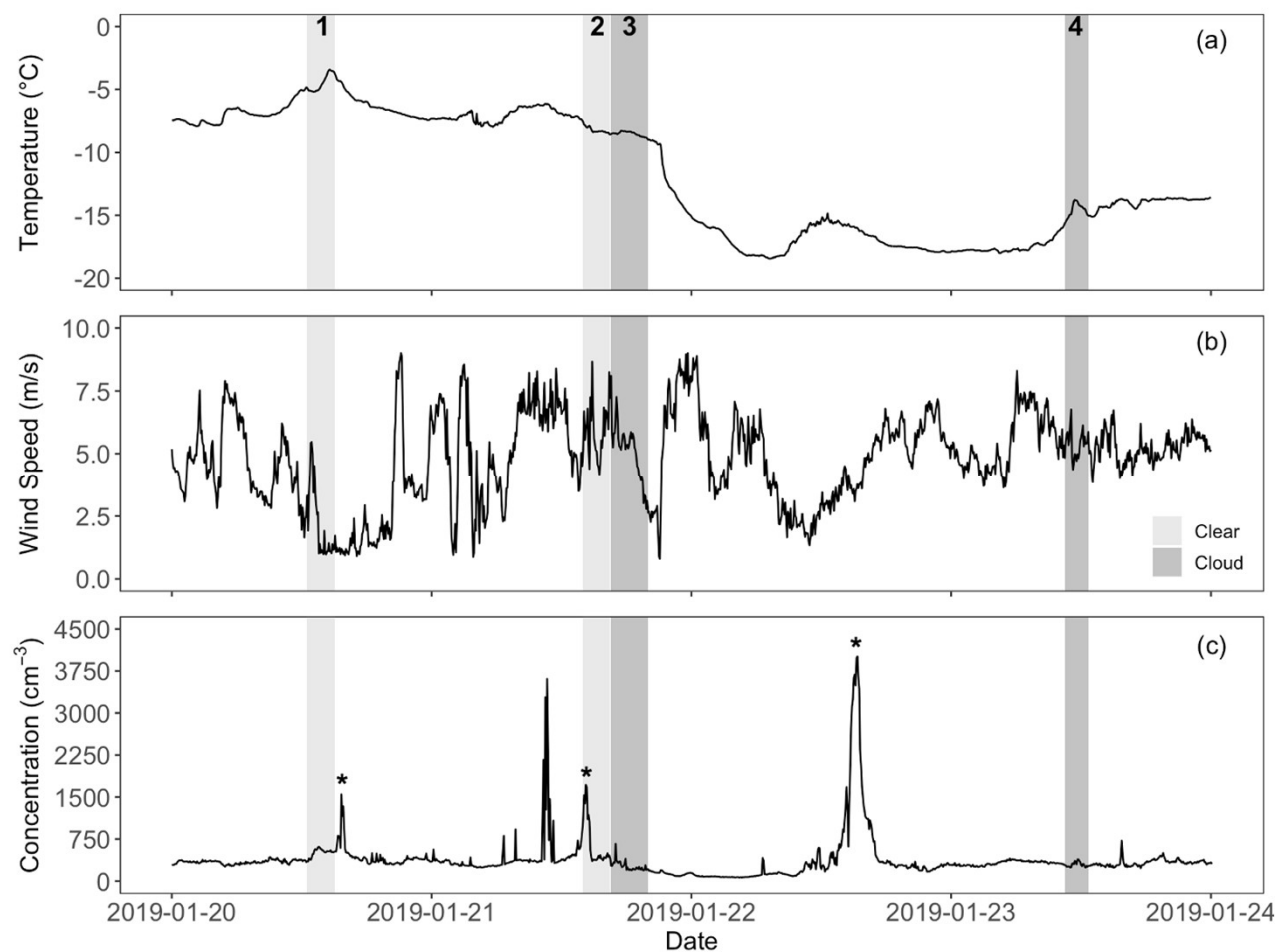
Figure S6: Meteorological conditions during sampling periods at SPL. (a) Temperature; (b) Wind Speed; (c) SMPS background concentration at SPL during the study period. Asterisks denote possible new particle formation. Other spikes are most likely caused by snow machinery. Light gray areas represent clear conditions, dark gray areas represent cloudy conditions.
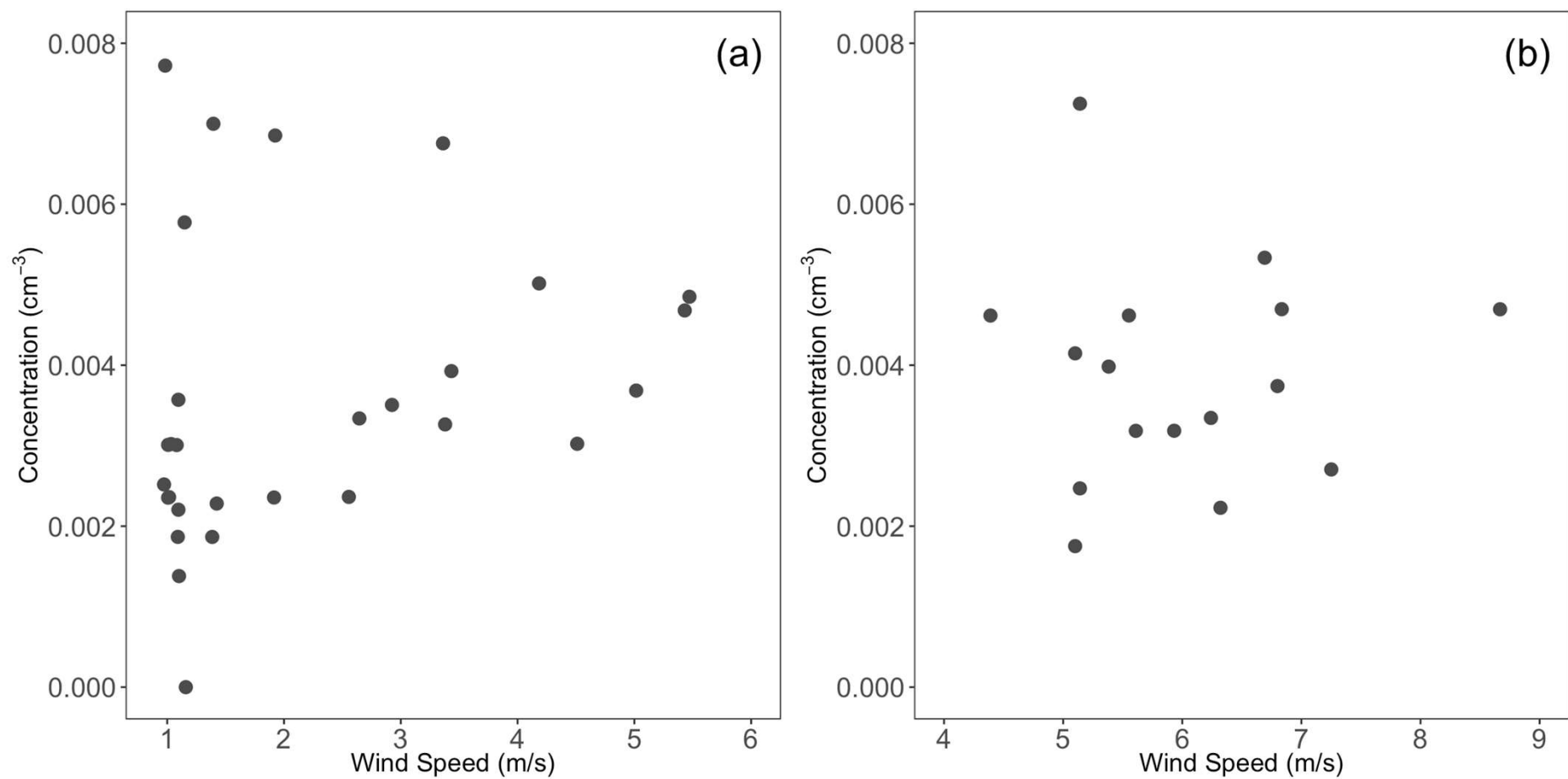
Figure S7: Ice crystal residual particle concentration as a function of wind speed during clear periods: (a) period 1, 1/20/2019; (b) period 2, 1/21/2019.